# RSC Advances

ROYAL SOCIETY OF CHEMISTRY

www.rsc.org/advances

Journal Name

RSC Advances

**ARTICLE TYPE**

# All Solution-based Processes for Fabrication of Superstrate-type configuration CuInS₂ Thin Film Solar Cells

**Amir Hossein Cheshmekhavar[a], Ali Reza Mahjoub[a,*], Hanieh Fakhri[a] and Mahdi Dehghani[b]**

CuInS₂ (CIS) thin films have proven as promising candidates for photovoltaic technology but still cost and safety of fabrication processes remain as challenging topics for research and development. Our effort is based on avoiding the costly vacuum-based deposition methods that use selenization and high temperature processes. The cadmium free cell structure <Glass/FTO/TiO₂/In₂S₃/CIS/carbon> was 
10 fabricated using a CuInS₂ nanocrystal ink at low temperature and without selenization or sulfurization steps. All used processes have been non-vacuum and solution based. To form a stable ink, Surfactant and binder-free monodispersed CIS nanocrystals were synthesized via ~~by a~~ hot injection method in ethylene glycol solvent and re-dispersed in DMF. Spray pyrolysis method was used for deposition of TiO₂ and In₂S₃ as blocking and buffer layers, respectively. Doctor Blading method was used to coa~~ting~~ CIS films on the buffer layer. The final CIS absorber layer was achieved after heat treatments at 150 and 250 ˚C, without any selenization process. Amount of carbon 
15 residue in final CIS film has been very low (~3%). Effective parameters on photovoltaic performance including type of sulphur source, buffer-layer thickness and CIS grain size and morphology were optimized. The optimum superstrate-type solar cell device showed promising power efficiency up to 3%.

## 1. Introduction

20 Among natural resources, solar energy provides clean energy and low price source that has been widely employed to generate electric power in public facilities. Nowadays, chalcogenides have attracted a great deal of attention as potential absorber candidate for thin layer technology. [1-4] Within the chalcogenide family, 
25 CuInS₂ (CIS) is introduced to be a promising choice as an absorber layer in thin film solar cells due to its large light absorption coefficient and direct band gap (1.5 eV) that is well match with the visible region of solar spectrum. [5-9] Currently, the solar cell efficiency of 11.4% for CIS has achieved by a vacuum 
30 based preparation technique. [10] However, high efficiency polycrystalline thin-film CIS solar cells require to deposition of absorber layer by vacuum deposition techniques such as evaporation and using of sulfur or selenium atmosphere at high temperature. [11-14] In spite of the high efficiency and good 
35 crystallinity of products in vacuum-based methods, three factors, high production cost, material waste and using of toxic element (selenium), have limited development of the CIS solar cell in large scale. [15-17] The key factor to develop the power generation with CIS solar cell is reducing the power generation cost. 
40 Nowadays, there is great interest in the expanding of low-cost processing methods for the growth of high-quality CIS-type absorbers for thin film solar cell applications. Over the past years, many efforts were focused toward the non-vacuum deposition method and using of superstrate-type configuration for CIS solar 
45 cell. Although power conversion efficiency is very limited in these techniques. [17-21] Among the main categories of non-vacuum

approach for deposition of inorganic absorber layer, solution based processes is one of the well technique that offer great potential for simple fabrication methods and low cost 
50 photovoltaic device solar cells. This approach is based on the Printing/coating from precursor solutions ink [22-23] or nanoparticles ink. [24-25] Superiority of precursors ink is its simple preparation. But it has some obstacles: the ink is very unstable, and using of organic binders to get suitable rheological properties 
55 for coating in these inks leads to incomplete decomposition of the organic content and carbon residue in the absorber film, resulting in shunt or recombination centres. [26-27] Nanoparticles inks are prepared with synthesis of CIS nanoparticles, followed by extraction, washing and re-dispersion in a suitable solvent. This 
60 technique allows purification of the ink trough washing and extraction steps. [28] In other hand, stability of nanoparticles ink is better than precursor ink. In general, the stability and homogeneity in the nanocrystal composition and size are two important parameters for preparation a suitable ink. However, in 
65 many nanoparticle ink reports are used from surfactant or stabilizer to control of composition or viscosity of the ink. But for high efficiency devices and low cost printing in large scale removal of these surfactants or stabilizer is necessary. [29-30] Investigation of high efficiency solution based processes shows 
70 the most reports are related to approachs that use from hydrazine as solvent . But hydrazin has several problems. This solvent is very toxic and hazardous. In other hand, many metal precorsurs hardly solve in this solvent or are insoluble. [31-33] Polyalcohol systems (like EG, DEG, TEG) are low cost and less

toxic and metal precursors like cupric salts and indium salts have much larger solubility in these systems, leading to higher yield. [34-35] Here, we have used ethylene glycol (EG) and metal chloride as a solvent and metal precursurs, respectively, to

5 surfactant- and binder-free synthesize CIS via a hot injection route. Also we have investigated effect of sulfur source on quality of the ink. The ink was formed by extraction of nanoparticles and followed by redispersing in DMF. Final CIS ink was used as absorber layer in a totally solution processed CIS solar cell with

10 superstrate-type configuration at atmospheric condition. Our effort is based on avoiding the costly vacuum-based deposition methods that use selenization and high temperature processes. The cadmium free cell structure <FTO/TiO$_2$/In$_2$S$_3$/CIS/carbon> was fabricated at low temperature and without selenization or

15 sulfurization step. For optimizing the cell performance, relationships between the photovoltaic performance and the synthetic/geometric parameters (e.g., CIS annealing temperature, buffer-layer thickness, distance between spray nozzele and film surface) were investigated. The resulting CIS thin films showed

20 promising power conversion efficiencies up to 3%.

**Experimental Section**

*2.1. Materials*

Cupper (I) chloride (CuCl, 99.99%), Indium (III) chloride (InCl3, 99.99%) were purchased from Sigma Aldrich. Thiourea

25 (CH$_4$N$_2$S, 99.99%), thioacetamide (C$_2$H$_5$NS, 99.99%), ethylene glycol (C$_2$H$_6$O$_2$), tetraisopropyltitanate, acetyl acetone, ethanol and N, N-Dimethylformamide (DMF) were purchased from Merck. All chemicals were used without further purification.

30 *2.2. Synthesis method*

CuInS$_2$ nanoparticles were synthesized via hot injection technique. A typical synthesize procedure was performed under atmosphere of Argon in order to purged of water and oxygen during the reaction. The experimental procedure was arranged in

35 brief: 0.9 mmol of Cupper (I) chloride (CuCl) and 1 mmol of Indium (III) chloride (InCl$_3$) were dissolved into 12 ml ethylene glycol in a 100 mL three-neck flask under Ar atmosphere. Subsequently, they were mixed together for 45 min at 120 ˚C. At the same time 5 mmol of thiourea was separately dissolved in 6

40 mL of ethylene glycol under an Argon atmosphere at 100 ˚C. The Cu/In/S ratio was adjusted to 0.9/1/5 to obtain Cu-poor and S-rich stoichiometry. After preparing two solutions, the thiourea solution was slowly injected into the first solution. After that, the temperature of reaction mixture was quickly increased to 200 ˚C

45 and the colour was changed from sky-blue to colourless and finally to black. The black colour appearance can be due to the formation of CuInS$_2$ nanoparticles. The reaction mixture was refluxed under Argon flow for 60 min at 200 ˚C. Afterward, then solution mixture was cooled down to the room temperature. The

50 obtained colloidal solution was then centrifuged at 8300 rpm for 15 min, the upper layer liquid was decanted, and the isolated particles were washed with ethanol. Dispersion of the final nanoparticles in DMF solvent formed a viscous and stable ink which can be easily deposited onto substrates. For further study,

55 the sulfur source was altered from thiourea (TU) to thioacetamide (TAA) and thiosemicarbazide (TSC).

*2.3. Device fabrication*

CIS solar cells were fabricated in a superstrate-type configuration

60 <FTO/TiO$_2$/In$_2$S$_3$/CIS/carbon>. The FTO (15 Ω/ cm$^2$, Dyesol) was first put in a bath with soap and water. After that, it was cleaned prior to film deposition by ultrasonication for 15 min in HCl, ethanol and acetone solvents, and followed by heat cleaning at 500 ˚C. A TiO$_2$ dense blocking film (~100 nm) was deposited

65 by spray pyrolysis method at 450 ˚C from a solution containing ethanol, acetyl acetone and titanium tetraisopropoxide (TTIP) as previously reported. [36] The spray solution was obtained by dissolving 0.72 mL TTIP and 0.108 mL acetyl acetone in 15 mL ethanol. Aluminium nozzle and sensor hot plate were used to

70 spray processes and controlling of temperature. The samples were placed on a hot plate in air by preserving the surface temperature around 450 ˚C. The surface temperature is critical and should be uniform over the sample. The other critical parameters in spray method are the distance between the nozzle of the nebulizer, and

75 the ~~hot~~ surface temperature of the samples. In spray pyrolysis method, the droplet size is an important factor. Spray in large distance leads to non-uniform films with poor adhesion because of forming solid nanoparticles and precipitate onto the hot surface, results in a nanoporous film. If the distance between the

80 nozzle and the hot plate is small the droplets have not fully evaporated ~~and~~ but precipitated, like rain drops, on~~to~~ the surface. The quality of obtained layers are low, since the adhesion is poor and usually many pinholes are formed. The desired deposition regime lies between these two extremes. [37-38] Noting to

85 mentioned points, the desire distance between the nozzle of the nebulizer and the hot plate was 22 cm. Also for setting the spray speed, we used from air compressor and the spray speed was adjusted 1 mL/min. After spray deposition, the films were kept at 450 ˚C for 60 min.

90 In$_2$S$_3$ buffer layer was coated onto the surface of the TiO$_2$ compact layer using the spray method. An aqueous solution of InCl$_3$.4H$_2$O and thiourea was used to deposit In$_2$S$_3$ film on TiO$_2$ layer. These materials with a molar ratio (In:S) of 1:6 were solwly dissolved in 6 ml distilled water. The concentration of

95 In$_2$S$_3$ precursor solution was 0.25 mol/L. The spray of solution was carried out with the speed of 4 ml/min at 350 ˚C and the distance between nozzle and film surface was maintained at 18 cm. Finally, the films were cooled to room temperature.

In the next step, The CIS nanocrystals films were deposited by

100 simple knife coating. Typically, a small amount of the concentrated CIS nanocrystal ink is was dropped at one edge of In$_2$S$_3$ buffer layer. A glass rod ~~is~~ was then swept towards over the substrate to create a uniform coating. The as-deposited films were then placed on a preheated 150 °C hot plate for 10 min. Without

105 cooling, the heated sample was immediately moved to a preheated 250 °C hot plate and maintained at this temperature for 10 min until the solvents and anions were removed by thermal evaporation and decomposed by air annealing, respectively. After heat treatment, the samples were allowed ~~to~~ be cooled to room

110 temperature in an air environment. At the end, thin film was covered by a layer of carbon polymer (Sharif Solar) as the back contact and then dried in oven at 120 ˚C for 20 min. The total active area was 0.16 cm$^2$. The J–V measurement was operated under simulated Air Mass 1.5 global illumination.

115 *2.4 Characterization*

The crystal structural properties were determined by X-ray
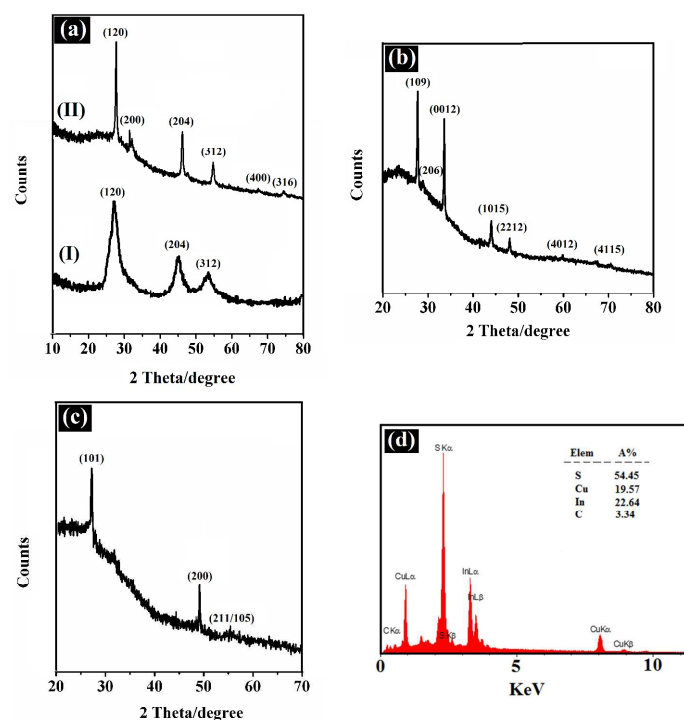
**Fig. 1** (a) The **XRD** patterns of as prepared CIS nanoparticles by hot injection method in 200 ˚C (I) and annealed CIS film at 250 ˚C for 10 min (II). (b) The **XRD** pattern of the $In_2S_3$ buffer layer. (c) The **XRD** pattern of the $TiO_2$ compacet layer. (d) Typical **EDS** pattern of the CIS film after annealing at 250 ˚C.

diffraction (XRD) using philips X-pert X-ray diffractometer using Cu Kα radiation (wavelength, λ = 1.5418 Å). The SEM images of the films were taken using Philips XL-300. Fourier transform infrared (FT-IR) spectra were determined on a
5 Shimadzu-8400S spectrometer in the range of 400-4000 cm$^{-1}$ using KBr pellets. The diffuse reflectance spectroscopy (DRS) was achieved using Shimadzu-UV-2550-8030 spectrophotometer. The optical properties of the deposited layers were determined by measuring the transmittance and absorbance spectra by
10 Shimadzu-UV-2550-8030 spectrophotometer in the range of 190-1000 nm. The performance of the solar cells were measured using a solar simulator (Sharif Solar) equipped with a source meter (Keithely 2400). The power of the simulated light was calibrated to AM 1.5 (100 mW/cm$^2$) using a standard photo diode. The cells
15 were characterized under a mask by covering the glass edges.

## 3. Results and discussions

### 3.1 CIS film characteristics

Improvment of rheological proprties and homogeneity in the nanocrystal composition and size are basic parameters for
20 preparing a suitable ink in the sulfide nanocrystal thin film deposition method. A huge barrier for achievement to a suitable ink formulation is using of various organic ligands, surfactants, or stabilizers, which are difficult to remove post-film coating. In this study, we tried to develop the surfactant and binder free synthesis
25 method for preparation CIS nanoparticles ink. Finally, prepared ink were used in a cost effective coating method. Using a suitable solvent that has functional group which can effectively stabilize nanocrystals and acts as capping agent, is the critical factor for preparation a nanocrystal ink. Accordingly, N,N-

30 Dimethylformamide (DMF) is was chosen as a suitable candidate for in this work because its functional groups can stabilize the nanocrystals effectively. We have used no binder, surfactant or stabilizer to prepare our nanocrystal ink because of the strong coordination effect of DMF functional group. In the other hand,
35 due to DMF moderate boiling temperature (150–154 ˚C), organic residual of solvent in the final coated thin film, can be easily removed by a mild heating treatment in the air. After re-dispersing the CIS nanocrystals in DMF (200 mg/ml), a viscose ink was achieved that can be applied directly on $In_2S_3$ buffer
40 layer.

### 3.2. The structural description of product

The XRD pattern of as-prepared CIS nanoparticles by hot injection method in 200 ˚C is shown in Fig. 1a, I. The pattern
45 indicates the as-prepared product is has crystalline structure. All diffraction peaks can be indexed as the pure chalcopyrite phase of $CuInS_2$ by comparison with data from JCPDS file no. 750106. Bragg's reflections for CIS NPs are observed in XRD pattern at 2θ values of 27.97˚, 46.43˚ and 55.16˚ indicated the presence of
50 chalcopyrite crystals. Based on the XRD results, there are no peaks of the other impurity phases such as CuS and $In_2S_3$ . So the pure phase of chalcopyrite CIS is achieved. Fig. 1a, II shows the XRD pattern of the CIS film deposited on soda lime after thermal treatment at 250 ˚C. The XRD pattern of resulting product closely
55 matches closely with the characteristic peaks of chalcopyrite phase of $CuInS_2$ (JCPDS No. 750106). The diffraction peaks at 2θ values of 27.97˚, 32.40˚, 46.43˚ 55.16˚, 67.90˚ and 74.88˚ are assigned to (120), (200), (204), (312), (400) and (316) planes of chalcopryte CIS phase. The XRD pattern revealed sharp peaks,

indicating the high degree of crystallinity. Furthermore, no characteristic peak related to the impurities can be found in the XRD patterns, and as a result, the XRD data shows that only CIS phases exist in the films. The XRD pattern of the CIS film after second annealing at 250 ˚C shows stronger peak intensities compared to as-prepared CIS nanoparticles that it indicates better crystalinty for annealed film than as prepared nanoparticles, resulting in improvement of $Jsc$ and the FF.

The possible formation mechanism of nanocrystalline $CuInS_2$ is proposed based on the experimental results. In this work, chloride salts of metals and thiourea were dissolved in ethylene glycol as metals precursor and sulfur source, respectively. After solving of metal precursors up to 100°C, the formation of Cu-EG and In-EG complexes can be detected by changing in the solution colour that are shown by proposed Equations 1 and 2. The solution colour was sky blue up to 100°C due to the formation of copper complex:[39]

$$CuCl + C_2H_6O_2 \rightarrow [Cu (EG)]^{1+} \qquad (1)$$
$$InCl_3 + C_2H_6O_2 \rightarrow [In (EG)]^{1+} \qquad (2)$$
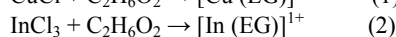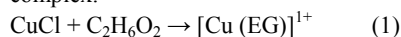
When the temperature exceeded 100°C, the colour changed to dark bluish green. The solution colour changed to light green at 120 °C because of the formation of indium complex. In the second flask, by solving thiourea the solution was transparent. Subsequently with increasing temperature more than 150°C, the complexes of Cu- EG and In-EG were decomposed to produce copper and indium ions and solution changed to colorless. In this temperature, injection of sulfur source into a copper and indium solution could be resulted in the nucleation of the nanocrystalline along with their growth. At about 200°C, the smoke began to evolve and the colour turned from transparent to brown and finally to black which indicates that complexes decomposition followed by the nucleation of nanocrystals.

$$Cu^+ + In^{3+} + S^{2-} \rightarrow CuInS_2 \qquad (3)$$
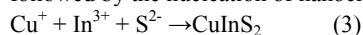
The extra ethylene glycol and thiourea play the role of capping agent via reacting hydroxyl (OH⁻) ligand with nanoparticle surface.

Fig. 1b shows the X-ray diffraction pattern of the $In_2S_3$ buffer layer derived from the spray of 6 ml $InCl_3.4H_2O$ and tiourea aqueous solution at 350 °C for 1.5 min. All the resultant products displayed the characteristic XRD peaks corresponding to face-centered cubic structure of $In_2S_3$, according to the JCPDS card no. 25-0390. No XRD peaks arising from the possible impurities such as $In_2O_3$, InS, and other phases of $In_2S_3$ were visible, suggesting the formation of pure cubic phase of $In_2S_3$.

Fig. 1c indicates the XRD pattern of the $TiO_2$ compact layer that is deposited by spray pyrolysis method at 450 ˚C. The XRD peaks for $TiO_2$ at 26.6˚, 44.2˚, and 52.3˚ are indexed to (112), (220/204), and (321/116) reflections of the anatase structure, in which the observed peaks match well with the reference JCPD data (JCPDS card no.21-1272).

Fig. 1d illustrates the typical EDAX pattern of the $CuInS_2$ film after annealing at 250 ˚C. For each sample, EDAX was taken from different points on the surface and their mean value was reported as the actual composition. The ratio of Cu:In:S is close to 0.9:1:2, which is obviously inconsistent with the Cu-poor CIS. As it can be seen the percentage of carbon in final film is very low comparable to previous reports. [40-43]A large problem in coating/printing of thin layers is presence of carbon impurity in final film that it can cause shunt paths across the film. Therefore, charge recombination is enhanced and open circuit voltage ($V_{oc}$) of the solar cell device is diminished. In other hand, exiting of organic residues in the film duo to thermal treatment, influences on increasing voids and cracks in the final film. Considering that the Cu:In:S precursor ratio was 0.9:1: 5 in start materials, an excess S in the precursor solution may have been lost during the sintering process in the air environment. Compared to stoichiometric ratio, excess thiourea have been used to avoid the formation of a white precipitate related to Cu-thiourea complex. [44] In other hand, we have used cu-poor stoichiometry because it is an important parameter in the chemical composition of final film to obtain highly efficient solar cells. The Cu-poor films have two advantages: (i) avoiding of the formation highly conductive unfavourable impurity phases such as $Cu_{2-x}S$, $Cu_3S_2$, and CuS, consequently not needing to toxic KCN post-treatment step. (ii) Improvement the semiconducting properties, such as charge carrier mobility and carrier concentration. [45-46]

Fig. 2a indicates SEM image of CIS sample prepared with thiourea as sulfur source. The image shows particle morphology, that is a typical morphology for the low temperature approach. Nanoparticles are relatively uniform in size with an average particle size of 50 nm and standard deviation of 3.2 nm. The histogram of the particles size distribution for the obtained product has been illustrated in Fig. 2a using microstructure measurement program and Minitab statistical software. Fig. 2b shows a cross sectional SEM of the CIS film annealed at 250 ˚C for 10 min. There is no crack in the as-deposited thin film during the drying procedure, and the layer is roughly 1.8 μm thick. It can be seen from Fig. 2b heating the CIS film at 250°C leads to produce a structure that has some voids, possibly resulting from decomposition of volatile surface ligands and precursor materials. In the other hand, the particles fused together and composed a well-connected network that is important for efficient carrier transport. [47] Also, crystal growth due to thermal treatment is clearly observed. The size of particles is up to 200 nm which is larger than previous works for low temperature device fabrication without selenization step. [17-19] Fig. 2c, d shows SEM images of spray deposited $TiO_2$ and $In_2S_3$ films respectively. The packed film shows uniform thickness with no pores or cracks These layers were achieved by optimizing precursor concentration, spray time and nozzle distance to the hot plate.
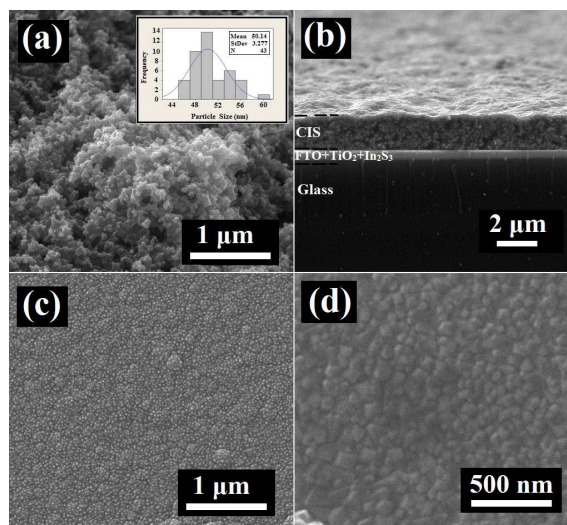
**Fig. 2** (a) **SEM** image of CIS sample prepared with thiourea as sulfur source with the statistical graph of particle size distribution of CIS nanocrystals prepared in the optimal conditions in the inset and (b) Cross sectional **SEM** of the CIS film annealed at 250 ˚C for 10 min. (c) **SEM** image of spray deposited $TiO_2$ blocking layer. (d) **SEM** image of spray deposited $In_2S_3$ buffer layer.

FT-IR spectra of the final annealed film at 250 ˚C clearly evidence the purity of the final CIS film. The characteristic vibrations at 3417 cm$^{-1}$ ($v$(OH)), proves the presence of moisture on the surface of CIS film. There are no peaks in the range of
5 4000-400 cm$^{-1}$, which proves the annealed CIS film doesn't have IR-active impurities (Figure 3a). The organic molecules were removed by washing with ethanol and thermal treatments.

Because the deposition of CIS was carried out under air conditions at low temperature, Raman analysis was used to reveal
10 the presence of secondary phases such as metal chalcogenides including $In_xS_y$ and $Cu_xS_y$, which are not well distinguished in XRD analysis. The Raman spectrum of CIS film is shown in Fig. 3b. The dominating CIS Raman peaks were detected at 290 cm$^{-1}$

and 340 cm$^{-1}$ are related to the $A_1$ and $B_2$ modes of chalcopryte ordering. The XRD and Raman analysis results indicate the purity of the final CIS absorber phase.
40 XPS survey spectrum analysis of CIS film prepared from nanoparticles inks is shown in fig. 3c. The XPS data shows following impurities on the top surface of the film: Cl= 1.5%, C= 5.5%, N= 0.4% and it shows Cu/In=0.92. XPS is a surface analysis technique and the data is not necessarily applied for the
45 bulk. XPS data also shows slight amount of oxygen on the surface which is expected with our air annealing of the films.

*3.3 Effect of sulfur source*

The CIS nanoparticles were prepared by refluxing ethylene glycol
50 solution containing CuCl, $InCl_3$ and several sulfur sources. XRD patterns of obtained $CuInS_2$ using thioacetamide and thiosemicarbazide as the sulfur source are reported in Fig. 4. In terms of phase identification, all of the diffraction peaks are matched well with the chalcopyrite phase with pattern (JCPDS
55 No. 750106). This fact confirms that the nature of sulfur source did not influence on the phase of the final product.
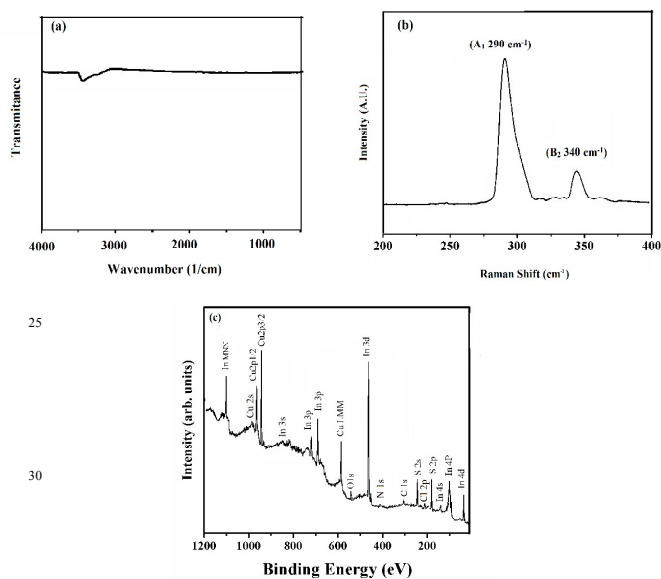


**Fig.3** (a) **FT-IR** spectra of the as-prepared nanoparticles and CIS film annealed at 250 ˚C. (b) **Raman** spectrum of the CIS film after annealing at 250 ˚C for 10 min. (c) XPS survey spectrum analysis of CIS film prepared from inks. The films were dried at 150 °C for 10 min and then annealed at 250 °C for 10 min.
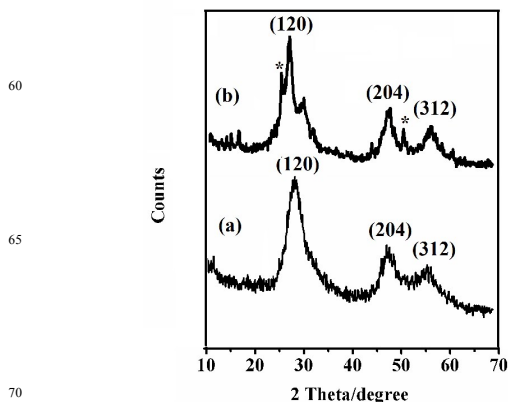


**Fig.4** The **XRD** patterns of as prepared CIS nanoparticles by thioacetamide (a) and thiosemicarbazide (b) as sulfur source.
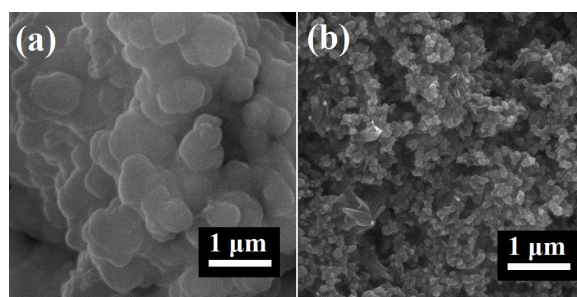
**Fig. 5 SEM** image of CIS sample prepared with thiosemicarbazide (a) and thioacetamide (b) as sulfur source as sulfur source.

In the case of thioacetamide, no diffraction lines of impurities were identified in the XRD pattern and intensity of the peaks can be implied to relatively good crystalline nature of this product (Figure 4a). But, when the TSC was employed as a sulfur source, there are diffraction lines of impurity phases (Figure 4b). A peak at 25.9◦ and 52.9◦ in the XRD pattern could be attributed to the forming of CuS (JCPDS card no 06-0464). [48] Despite synthesized samples with different sulfur sources have same XRD pattern but an influence on peak width and, consequently, on the crystallite size of CuInS$_2$ nanoparticles was observed.

The intensities of three main peaks of (120), (204) and (312) planes suggest that the crystal size in synthesized samples with various sulfur sources is are different. The results show the crystal growth of CIS with thiourea, is higher (Figure 1a), than thioacetamide and thiosemicarbazide as sulfur sources (Figure 4a, b). The XRD results show that TSC may not be a proper sulfur source to stnthesize CIS nanoparticles under arranged conditions of hot injection. Many studies on ternary I–III–VI$_2$ show that the shape and the size of final product depend on the reaction solvents or surfactants. In this work, it was interesting that the size of as-prepared CIS nanoparticles were strongly influenced by the type of the sulfur sources.

Fig. 5 shows the effect of sulfur source on the shape and particle size. It is clear that sulfur source plays an effective role in controlling size of products. Since the reactivity of different sulfide sources is not the same in the coordination reactions, synthesized CuInS$_2$ particles using different sulfide sources varies in the shape and size. As can be seen by using TSC as the sulfur source, the particles were agglomerated (Figure 5a). It can releases sulfide ion quickly. [49] Therefore the sizes of particles were small, and small particles were fused to each other and the large particle size is obtained for this product. When TAA was used as sulfur source the particles size was around 90 nm. In case of TAA, the sulfur can be released more slowly, and the rate of growth was more than creating nucleus and the large particles were achieved. However, results suggested by altering of sulfur source from TAA to TU, synthesized nanopaerticles are uniform and the average particle size decreases of 90 nm to 50 nm.

*3.4 photovoltaic parameters*

The CIS layer tested as an absorber layer for a thin film solar cell device with the superstrate <SLG/FTO/TiO$_2$/In$_2$S$_3$/CIS (absorber layer)/back contact> structure. carbon polymer

was used as back contact. For deposition of CIS layer, we used nanocrystal

CIS ink prepared from redispersion of nanoparticles (synthesized by thiourea as sulfur source and reaction time of 60 min) in DMF. The current density versus voltage (J–V) characteristics was measured under 100 mW.cm$^{-2}$ illuminations. photovoltaic parameters such as $J_{SC}$ (the short-circuit current), $V_{OC}$ (the open-circuit voltage) and FF ( fill factor) , which are the significant factors to explain the performance of a solar cell device, were measured. For the optimum cell, the short-circuit current density, $J$sc, was 15.52 mA/cm$^2$, that was improved compared to previous reports for superstrate-type CIS solar cell devices. [17-21] The power conversion efficiency, $\eta$, the fill factor (FF) and open-circuit voltage ($V$oc ) were 3.03, 43% and 454 mV, respectively. The low open circuit voltage, which may be caused by recombination through the interface, the space charge region or the bulk of the absorber layer. [40] Meanwhile, we believe that this might be due to film voids. Organic residues from precursor can be exited in the second annealing of CIS film processes at 250 °C, resulting in production a structure that has some voids.

Fig. 6a shows the current-voltage diagrams of the cells fabricated by using different sulfur sources based ink formulations. The results suggest that type of sulfur sources highly influences both the $J_{sc}$ and $V_{oc}$ of the devices. By altering sulfur source from TU to TAA, both of the current density and open-circuit voltage are diminished. For TSC, the results were disappointed and the $J$sc and $V$oc were negligible (Table 1).

**Table 1**. The device performance parameters for CIS cells fabricated using nanocrystals inks based different sulfur sources. Here, TU represents thiourea, TAA represents thioacetamide and TSC represents thiosemicarbazide.

| Sulfur source | Buffer layer deposition | $J_{sc}$ (mA/cm$^2$) | $V_{oc}$ (mV) | FF (%) | Efficiency (%) |
|---|---|---|---|---|---|
| TU | Spray | 15.52 | 0.454 | 43 | 3.03 |
| TAA | Spray | 8.67 | 364 | 42 | 1.36 |
| TSC | Spray | 3.71 | 359 | 29 | 0.64 |
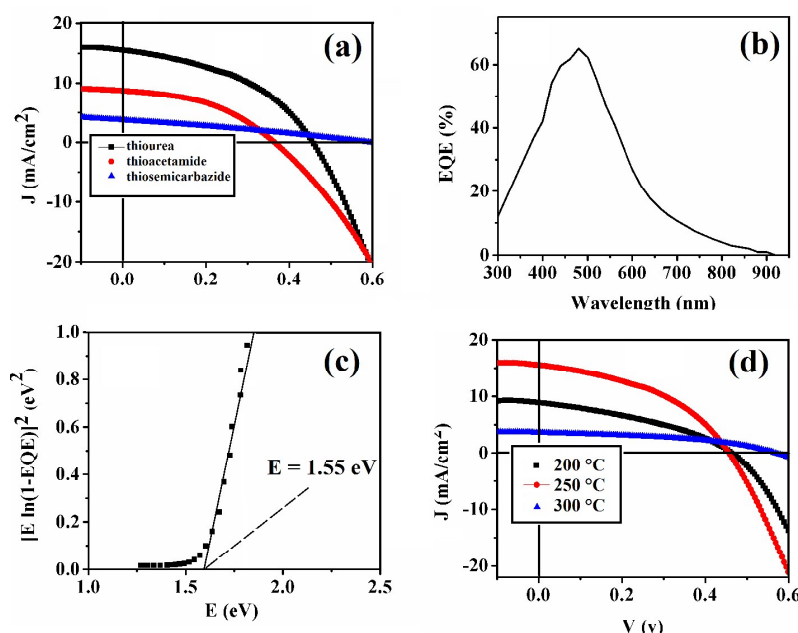
**Fig. 6** (a) Current-voltage diagrams of the cells fabricated by using different sulfur sources based ink formulations. (b) External quantum efficiency (EQE) of the champion CIS solar cell. (c) Bandgap ( Eg ) determination of the device from the EQE data  (d) **J−V** curves obtained from the device prepared at various annealing temperatures.

The final morphology of the CIS film is the esential reason for the contribution of sulfur source in the ink. For TU based inks, a rather dense and uniform layer is formed (Figure 2), while this is not the case for TAA and TSC inks where the layers show voids and porosity (Figure 5).  Morphology plays a critical role in solution processed solar cells, by affecting defect density and recombination. All of three sulfur sources operate as sulfur source and also as capping agent to form the product. The number of $NH_2$ functional groups connected to C= S agent in TAA is less than TU and TSC. Therefore, the probable coordination manner of TAA to metal ions is restricted, while TSC and TU molecules have a strong tendency to coordinate with metal cations and easily form the precursor complexes. The nucleation and growth play critical roles in particle size of final product. In the case of TAA, the release rate of sulfur is lower than TU and TSC, so rate of growth was superior. Consequently, larger particles were obtained in comparison with TSC (Figure 5). Since the TSC molecules which have the more $NH_2$ functional groups than TAA and TU, can immediately release sulfur, so the rate of nucleation will be greater than growth. Therefore the sizes of particles were small, and small particles fused together, consequently a sponge shape morphology was attained for this sulfur source. With changing sulfur source to thiourea, the rate of nucleation and growth became optimum and separated microspheres with small particles were achieved.

Fig. 6 b shows the external quantum efficiency (EQE) response from a CIS superstrate solar cell fabricated using a nanoparticles Ink. Jsc was calculated by convoluting the EQE response using the following equation:

$$Jsc = \int q \; \phi_{ph} \; EQE \; (\lambda)d\lambda,$$

Where, $\phi_{ph}$ is the spectral photon flux density of the AM 1.5 spectral intensity distribution as a function of the incident light wavelength  and q is the charge of the electron. [50] The calculated $Jsc$ value from the EQE spectra is 15.2mA/cm$^2$, close to the measured $Jsc$ value (15.52 mA/cm$^2$) obtained from the current density–voltage curve, as shown in figure 6(a). The EQE shows a maximum of ≈67% at a wavelength of 480 nm and extends up to 920 nm with a gradual decrease. The EQE decrease at higher wavelength and the appearance of a long tail at a wavelength above 600 nm and this suggests that bulk recombination is dominated in the absorber layer. This is related to insufficient crystallinity of the CIS films. This is partially due to the lack of high temperature sulfurization or selenization. The tail seen at wavelengths >700 nm is typically related to the presence of midgap states and shallow traps below the band edge.[47]

The bandgap determination of CIS layer from the long-wavelength ''absorption'' edge of the EQE curve is shown in fig. 6 c. The band gap was determined to be 1.55 eV by fitting a plot of [E ln (1 − EQE)]$^2$ against energy (E), which matches closely with the previous reported values for chalcopyrite CuInS$_2$ thin films. [51-53]

### 3.4.1 Effect of annealing temperature

The effect of the second annealing temperature on the quality of the CIS film and devices performances was investigated (Figure 6). Table 2 lists the photovoltaic parameters for different second annealing temperature of CIS film. The influence of annealing temperature was determined from samples with TiO$_2$ compact layer and In$_2$S$_3$ buffer layer with 100 and 60 nm thickness, respectively.

The best results were achieved from CIS annealing temperature at 250 °C with efficiency of 3.03%. An increasing of annealing
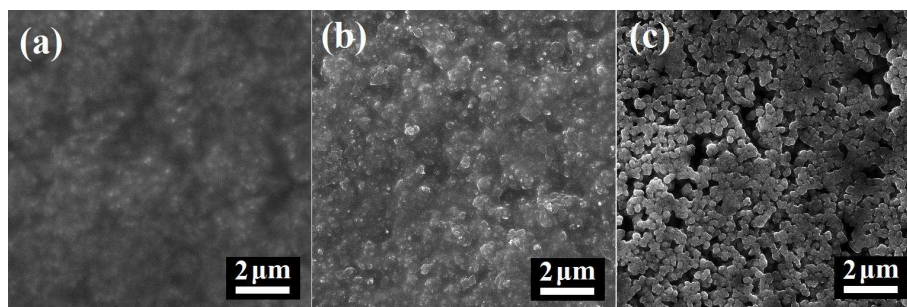
**Fig. 7** Top-view **SEM** images showing the morphological changes in the surfaces of CIS films prepared by printing of CIS nanocrystals ink at (a) 200ºC (b) 250 ºC and (c) 300 ºC.

temperature leads to increase of grain size (Figure7), results in photocurrent improvement. Improvement of ~~in~~ photocurrent related to reducing in grain boundaries, can significantly contribute to the formation of recombination centres. According to the data of Table 2, by increasing of annealing temperature from 200 to 250, the photocurrent density is increased from 8.82 to15.52 mA/cm². In other hand, the organic residues present in the as-prepared film, were removed by the second annealing process. Consequently, the numbers of voids were increased with the increasing annealing temperature (Figure 7). In substrate structure of CIS solar cells, filling of these voids with buffer during buffer layer deposition can help to charge carrier separation trough creating an interpenetrating heterojunction interface. However, in view of our cell configuration (Carbon/CIS/In$_2$S$_3$/TiO$_2$/FTO), the presence of pores allows to carbon penetrate in CIS layer and form shunt paths through direct contact with the In$_2$S$_3$ buffer layer, which in failing of cell performance. [47] When the second annealing temperature was increased above 250ºC device operation was deteriorated and the cell was showed a weak performance.

*3.4.2 Effect of buffer layer thickness*

N-type Wide band gap such as: CdS, ZnS and In$_2$S$_3$ were used as buffer layer in calchogenides solar cells.[17-21], cadmium sulfide was extensively used in high efficient CIGS solar cells. But, we have avoided this material because of presence of cadmium as a toxic and carcinogen element. We have used from In$_2$S$_3$ as buffer layer. As view of our cell configuration (Carbon/CIS/In$_2$S$_3$/TiO$_2$/FTO), the buffer layer plays the following roles:

(I) Improvement of the junction properties between the absorber and window layers.

(II) Preventing the formation of recombination centers such as interface traps and defect states.

(III) Protection of absorbing layer from mechanical and chemical damages.

(IV) Enhancing the thickness of depletion layer.

Here, Spray pyrolysis was used to deposition TiO$_2$/In$_2$S$_3$ layer. An In$_2$S$_3$ buffer layer was deposited to form a thin layer on TiO$_2$ packed layer and to form a p-n junction configuration using the p-type CIS as absorber layer. Results showed that the buffer layer thickness and quality has critical role in the device performance. The performance parameters for the devices with different In$_2$S$_3$ thickness are summarized in Table 3. We have not observed considerable photovoltaic response in absence of buffer layer that means electrons were not injected directly into the TiO$_2$ blocking layer without In$_2$S$_3$ buffer layer. The band gap of In$_2$S$_3$ is 2.1 eV [54] that is increased to 2.8 eV [55] for thin film of In$_2$S$_3$ with small grains contaminated with oxygen. The conduction bands of In$_2$S$_3$ and CuInS$_2$ are close together and have an offset of about 1 eV compared to the conduction-band energy of anatase TiO$_2$.[56] Therefore, electrons of conduction band can be easily injected into conductive band of TiO$_2$, which is located close to 4.2 eV,[57] through the interface between CuInS$_2$ and In$_2$S$_3$. Also, due to 1 eV energy gap, the back flow and returning to the CuInS$_2$ conduction band are impossible. In the other hand, TiO$_2$ and CIS physically separate with presence of 60 nm thin In$_2$S$_3$ buffer layer. Consequently, the recombination of conduction-band electrons of TiO$_2$ with valance-band electrons of CIS seems to be implausible. Therefore, with applying buffer layer both *Jsc* and *Voc* are improved. [58]

**Table 2**. The device performance parameters for the cells, with CIS film annealed at 200-300 °C. The optimum temperature lies between 200 °C and 300 °C.

| CIS crystallization temperature (°C) | $J_{sc}$ (mA/cm²) | $V_{oc}$ (V) | FF (%) | Efficiency (%) |
|---|---|---|---|---|
| 200 | 8.82 | 459 | 36 | 1.48 |
| 250 | 15.52 | 454 | 43 | 3.03 |
| 300 | 2.40 | 264 | 32 | 0.20 |

**Table 3**. The dependence of device performance on the deposition of In$_2$S$_3$ buffer layer.

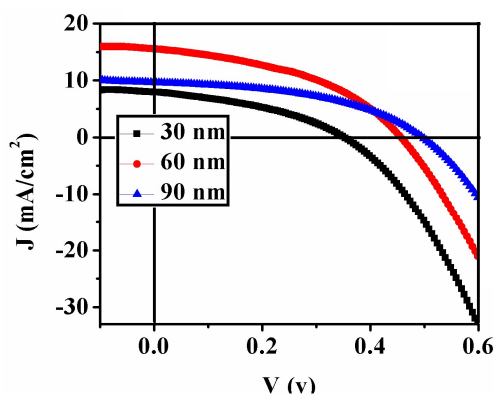| Thickness of In$_2$S$_3$ layer (nm) | $J_{sc}$ (mA) | $V_{oc}$ (mV) | FF (%) | Eff (%) |
|---|---|---|---|---|
| 0 | Device Failure | | | |
| 30 | 4.65 | 245 | 30 | 0.33 |
| 60 | 15.52 | 454 | 43 | 3.03 |
| 90 | 9.6 | 494 | 46 | 2.19 |

**Fig. 8** Illuminated **J−V** curves obtained from the photovoltaic devices prepared using spray pyrolysis over In$_2$S$_3$ buffer with different thickness.

The best device performance was achieved for an intermediate thickness (60 nm). This layer is packed and show uniform thickness (figure 2c). Compared with the other device parameters, open circuit voltage was changed with the altering of thickness of buffer layer. The In$_2$S$_3$ layer improves the junction properties between the absorber and window layers and prevents the formation of recombination centers such as interface traps and defect states.  Increasing in buffer layer thickness leads to increase of depletion layer thickness (where photogenerated charges are separated under a strong electric field, extended along either side of the p-type and n-type semiconductors), results in decreasing of interfacial recombination, enhancing of carriers density and better electron-hole separation. Consenquently, open circuit voltage was improved with a thicker In$_2$S$_3$ shell layer. In other hand, buffer layer with 60 nm thick showed high quality deposition (figure 2d). This layer provided a lower recombination probability during the efficient transfer of the generated charge carriers from the CIS to the In$_2$S$_3$ /TiO$_2$.
3.4.3

## Conclusions

In summary, a CIS nanocrystal ink was synthesized using a hot injection process by Copper (I) chloride (CuCl), Indium (III) chloride (InCl$_3$) and several sulfur source (TU, TAA and TSC) in ethylene glycol solvent. CIS nanocrystal ink was fabricated by extracting nanoparticles and re-dispersing in DMF. Purity of CIS layer was confirmed using FTIR, EDS and XRD analysis. In the final deposited film, the carbon content was negligible (about 3%). All solution-based CuInS$_2$ superstrate-type solar cell devices were fabricated at atmospheric condition and without selenization or sulfurization steps. Effective parameters on device performance such as type of sulfur source, annealing temperature, and buffer layer thickness were investigated. Results showed the rate of releasing sulphide ion influences on morphology and particle size of final product. Also, crystal growing and numbers of voids in final annealed film are related to second annealing temperature and therefore cause considerable Cu diffusion into the In$_2$S$_3$ buffer layer at high annealing temperature (higher 300 ˚C)  of 300 ˚C and higher, resulting in device failure. It was also found that the quality of the In$_2$S$_3$ buffer layer is critically important. It was also found that the open circuit voltage was increased with the enhancing of thickness of buffer layer because of decreasing of interfacial recombination, enhancing of carriers density and better electron-hole separation. The cell showed the optimum performance with a TU based ink and at 250 ˚C annealing temperature and with 60 nm thick of buffer layer. Conventional layered FTO/CuInS$_2$/TiO$_2$/In$_2$S$_3$/Carbon PV devices showed promising power conversion efficiencies up to ∼3%.

## Notes and References.

*$^a$Department of Chemistry, Tarbiat Modares University, P.O. Box. 14155-4383, Gisha Bridge, Tehran, Iran; Tel.: +98 21 82883442; fax: +98 21 82883455; E-mail: mahjouba@modares.ac.ir*

1   S. Seike, K. Shiosaki, M. Kuramoto, H. Komaki, K. Matsubara, H.Shibata, S. Ishizuka b, A. Yamada, S. Niki, *Sol. Energy Mater. Sol. Cells*., 2011, **95**, 254.
2   A. Virtuani, E. Lotter, and M. Powalla, U. Raub and J. H. Werner, M. Acciarri, *J. Appl. Phys*., 2006, **99**,014906.
3   P. O. Westin, U. Zimmermann, M. Ruth, M. Edoff, *Energy Mater. Sol. Cells.*,2011, **95**, 1062.
4   J. Palm, V. Probst, F. H. Karg, *Solar energy*., 2004, **77**, 757.
5   A. Cho, S. J. Ahn, J. H. Yun, J. Gwak, H. Song and K. Yoon, *J. Mater. Chem.*, 2012, **22**, 17893.
6   G. Norsworthy, C.R. Leidholm, A. Halani, V.K. Kapur, R. Roe, B.M. Basol, R. Matson, *Sol. Energy Mater. Sol. Cells*., 2000, **60**, 127.
7   X. Lu, Z. Zhuang, Q. Peng and Y.Li, *CrystEngComm*., 2011, **13**, 4039.
8   O. Kijatkina, M. Krunks, A. Mere, B. Mahrov, L. Dloczik, *Thin Solid Films*., 2003, **431 –432**, 105.
9   B. D. Weil, S. T. Connor,Y. Cui, *J. AM. CHEM. SOC*., 2010, **132**, 6642.
10  S. Siebentritt, *Thin Solid Films*., 2002, **1**, 403–404.
11  G. M. Ford, Q. Guo, R. Agrawal, H. W. Hillhouse, *Thin Solid Films*., 2011, **520**, 523.
12  Q. Guo, S. J. Kim, M. Kar, W. N. Shafarman, R. W. Birkmire, R. Agrawal, and H. W. Hillhouse, *Nano Lett.,* 2008, **8**, 9.
13  S. H. Chang, M. Y. Chiang, C. C. Chiang, F.W. Yuan, C.Y. Chen, B. C. Chiu, T. L. Kao, C. H. Laic and H. Y. Tuan, *Energy Environ. Sci.,* 2011, **4**, 4929.
14  Q. Guo, G. M. Ford, R. Agrawal, and H. W. Hillhouse, *Prog. Photovolt: Res. Appl*., 2012.
15  F. Long, W. M. Wang, H. Tao, T. k. Jia, X. M. Li, Z. Zou, Z. Fu, *Mater Lett*., 2010, **64**, 195.
16  D. C. Nguyen, K. Takehara, T. Ryo and S. Ito, *Energy Procedia*., 2011, **10**, 49.
17  J. W. Cho, S. J. Park, W. Kim and B. K. Min, *Nanotechnology*., 2012, **23**, 26540.
18  T. Ryo, D. C. Nguyen, M. Nakagiri, N. Toyoda, H. Matsuyoshi, S. Ito, *Thin Solid Films*., 2011, **519**, 7184.
19  M.R. Balboul, A. Jasenek, O. Chernykh, U. Rau, H.W. Schock, *Thin Solid Films*., 2001, **387**, 74.
20  L. Li, N. Coates, and D. Moses, *J. AM. CHEM. SOC*., 2010, **132**, 22.
21  M. G. Panthani, V. Akhavan, B. Goodfellow, J. P. Schmidtke, L.Dunn, A. Dodabalapur, P. F. Barbara,and B. A. Korge, *J. AM. CHEM. SOC.,* 2008, **130**, 16770.
22  A. Cho, S. Ahn,J.Yun, J. Gwak, S.K. Ahn, K. Shin,H. Song, K.H.Yoon, *Solar Energy Materials & Solar Cells*., 2013,**109**, 17.

23  S.Ahn, T. H. Son, A. Cho, J.Gwak, J. H. Yun, K. Shin, S. K.Ahn,S. H. Park and K. Yoon, *ChemSusChem.* 2012, **5**, 1773.

24  Q.Guo, G. M. Ford, R.Agrawal and H. W. Hillhouse, *Prog. Photovolt: Res. Appl.*, 2013, **21**, 64.

25  H.T. Tung, I.G. Chen, J.M. Song, M.G. Tsai, I.M. Kempson, G. Margaritondo and Y. Hwu, *Nanoscale.*, 2013, **5**, 4706.

26  Y. S. Lim, J.Jeong, J.Y. Kim, M. J.Ko, H. Kim, B. Kim, U.Jeong, and D.-K. Lee, *J. Phys. Chem. C*., 2013, **117**, 11930.

27  S. J. Ahn, C. W. Kim, J. H. Yun, J. H. Gwak, S. H. Jeong, B. H. Ryu and K. H. Yoon, *J. Phys. Chem. C.*, 2010, **114**, 8108.

28  A. Cho, S.Ahn, J. H. Yun, J.Gwak, H. Song and K. Yoon, *J. Mater. Chem.*, 2012, **22**, 17893.

29  K. Ramasamy, M. A. Malik, N. Revaprasadu and P. O'Brien, Chem. Mater., 2013, 18, 3551.

30  U. V. Ghorpade, M. P. Suryawanshi, S. W. Shin, C.W. Hong, I. Kim, J. H. Moon, J. Ho Yun, J. H. Kim and S. S. Kolekar, *Phys. Chem. Chem. Phys.,* 2015, **17**, 19777.

31  D.B. Mitzi, *Advanced Materials.,* 2009, **21**, 3141.

32  T. Todorov, D.B. Mitzi, *Eur. J. Inorg. Chem.* 2010, 17.

33  D.B. Mitzi, M. Yuan, W. Liu, A.J. Kellock, S.J. Chey, L. Gignac, A.G.Schrott, *Thin Solid Films.,* 2009, **517**, 2158.

34  X.Sheng, L. Wang, D. Yang, *J Sol-Gel Sci Technol*., 2012, **62**, 87.

35  H. Liu, Z. Jin, W.Wang, Y.Wang, H .Du, *Mater Lett*., 2012, **81**, 173.

36  M. Nanu, J. Schoonman and A. Goossens,  *Adv. Funct. Mater.,* 2005 **15**, 95.

37  M. Krunksa, O. Kijatkina, H. Rebane, I. Oja, V. Mikli, A. Mere, *Thin Solid Film*., 2002, **403 –404**, 71.

38  L.P. Deshmukh, R.V. Suryawanshi, E.U. Masumdar, M. Sharon, *Sol Energy.*, 2012, **86**, 1910.

39  P. ShengJie, L. Y. Liang, C. F. Yi, L. I. Jing, *Sci. China Chem.*, 2012, **55**, 1236.

40  D. Lee and K. Yong, *J. Phys. Chem. C.*, 2014, **118**, 7788.

41  C. Kind, C. Feldmann, A. Quintilla and E. Ahlswede, *Chem. Mater.*, 2011, **23**, 5269.

42  S. Ahn, T. H. Son, A. Cho and K. H. Yoon, *ChemSusChem.*, 2012, **5**, 1773.

43  U. Berner and M. Widenmeyer, *Prog. Photovolt: Res. Appl.*, 2014

44  J.C.W. Ho, T. Zhang, K. Lee, S.K. Batabyal, A.I.Y. Tok, *ACS Appl. Mater. Interface.*, 2014, 6, 6638.

45  P. Niyamakom, A. Quintilla,  K. K¨ohler, M. Cemernjak, E. Ahlswede and S. Roggan, *J. Mater. Chem. A*, 2015, **3**, 4470.

46  W.Septina, M.Kurihara, S. Ikeda, Y. Nakajima, T.Hirano, Y. Kawasaki, T.Harada and M. Matsumura, *ACS Appl. Mater. Interfaces*, 2015, **12**, 6472.

47  H.Azimi , T. Heumüller , A. Gerl , G.Matt , P. Kubis , M. Distaso , R.Ahmad , T.Akdas , M. Richter , W. Peukertand Christoph J. Brabec, *Adv. Energy Mater.,* 2013, **3**, 1589.

48  Y. Li, J. Scott, Y. Chen, L. Guo, M. Zhao, X. Wang, W. Lu, *Mater. Chem. Phys*, 2015 **162**, 671.

49  O. Amiri, M. Salavati-Niasari, M.Sabet, D. Ghanbari, *Materials Science in Semiconductor Processing*, 2013, **16**, 1458.

50  S. Merdes , R. SaezAraoz, A. Ennaoui, J. Klaer and R. Klenk, *Appl. Phys*. Lett., 2009, **95**, 213502.

51  H. Fakhri, A.R. Mahjoub, A.H. Cheshme Khavar, *Appl. Sur.Sci.*, 2014, **318**, 65.

52  B. Tell , J. L. Shay , H. M. Kasper , *Phys. Rev. B.,* 1971 , **4** , 2463.

53  H. W. Schock , *Sol. Energy Mater. Sol. Cells,* 1994, **34** , 19.

54  W. Rehwald, G. Harbeke, *J. Phys. Chem. Solids,* 1965, **26**, 1309.

55  N. Barreau, J.C. Berende. X. Castel, J. Pinel, *Solid State Commun.,* 2002, **122**, 445.

56  S. Siebentritt, *Thin Solid Film*, 2002, **403-404**, 1.

57  M. Gratzel, *Nature*, 2001, **414**, 338.

58  M. Nanu, J. Schoonman, A. Goossens, *Adv. Mater.*, 2004, **16**, 453

242x237mm (120 x 120 DPI)